Journal of Materials Science & Technology 87 (2021) 167–175

Contents lists available at ScienceDirect

Journal of Materials Science & Technology

journal homepage: www.jmst.org

Research Article

A fast numerical method of introducing the strengthening effect of residual stress and strain to tensile behavior of metal matrix composites

J.F. Zhang [a,b], X.X. Zhang [c,*], H. Andrä [c], Q.Z. Wang [a], B.L. Xiao [a,*], Z.Y. Ma [a]

[a] Shi-changxu Innovation Center for Advanced Materials, Institute of Metal Research, Chinese Academy of Sciences, Shenyang 110016, China
[b] University of Chinese Academy of Sciences, Beijing 100049, China
[c] Fraunhofer Institute for Industrial Mathematics, Fraunhofer-Platz 1, Kaiserslautern 67663, Germany

ARTICLE INFO

Article history:
Received 17 November 2020
Received in revised form
23 December 2020
Accepted 25 January 2021
Available online 19 March 2021

Keywords:
Metal matrix composites (MMC)
Finite element analysis (FEA)
Representative volume element (RVE)
Residual stress and strain
Aspect ratio

ABSTRACT

Thermal residual stress and strain (TRSS) in particle reinforced metal matrix composites (PRMMCs) are believed to cause strengthening effects, according to previous studies. Here, the representative volume element (RVE) based computational homogenization technique was used to study the tensile deformation of PRMMCs with different particle aspect ratios (AR). The influence of TRSS was assessed quantitatively via comparing simulations with or without the cooling process. It was found that the strengthening effect of TRSS was affected by the particle AR. With the average strengthening effect of TRSS, a fast method of introducing the strengthening effect of TRSS to the tensile behavior of PRMMCs was developed. The new method has reduced the computational cost by a factor 2. The effect of TRSS on continuous fiber-reinforced metal matrix composite was found to have a softening-effect during the entire tensile deformation process because of the pre-yield effect caused by the cooling process.

1. Introduction

Particle reinforced metal matrix composites (PRMMCs) are widely used in structural applications because of their high specific strength and stiffness [1–6]. With the increasing requirement of PRMMCs, a fast design method to predict the mechanical properties of new PRMMCs is in demand. The finite element (FE) simulation assisted composites material design method is developing and gaining more attention [7–13] in recent years.

To predict the mechanical properties of PRMMCs accurately, a deep understanding of their strengthening mechanisms is necessary. Because of the mismatch of thermal elastic and plastic properties between reinforcement and matrix, thermal residual stress and strain (TRSS) are generated inherently during heat treatment [14–16]. TRSS has been proved to be one strengthening mechanism of PRMMCs [17–20] and studied via the FE method by many researchers [21–27]. To check the effect of TRSS caused by the quenching process, the cooling process is usually modeled, which causes the initial stress and strain state prior to the loading process [28,29]. Since the cooling process simulation requires a coupled thermo-mechanical model and is very costly, it is crucial to find an efficient way to determine the effect of TRSS.

To analyze the effect of TRSS quantitatively, the strengthening contribution ratio of TRSS is defined by (as in Ref. [28]):

$$R_{\mathrm{TRSS}} = \frac{\sigma_{\mathrm{wc}} - \sigma_{\mathrm{oc}}}{\sigma_{\mathrm{oc}}} \tag{1}$$

where σ_{wc} and σ_{oc} are the predicted average tensile loading stress with and without the cooling process, respectively. Besides TRSS, load transfer and plastic strain gradient are also strengthening mechanisms of PRMMCs [28,29]. According to Ref. [28], for 15 vol.% SiCp/2009Al with 5 μm or 13 μm particles, the strengthening contribution ratios of load transfer and plastic strain gradient vary from 0% to 35% during tensile loading. Differently, the contribution ratio of TRSS is always less than 5% and almost not affected by the value of applied tensile strain or particle size. In summary, the contribution ratio of TRSS is relatively small and insensitive to tensile strain.

* Corresponding authors.
E-mail addresses: Xingxing.Zhang@frm2.tum.de (X.X. Zhang), blxiao@imr.ac.cn (B.L. Xiao).

https://doi.org/10.1016/j.jmst.2021.01.079
1005-0302/

To skip the simulation of the cooling process, the strengthening effect of TRSS on the average tensile loading stress can be obtained from Eq. (1):

$$\sigma_{wc} = (1 + R_{TRSS})\,\sigma_{oc} \tag{2}$$

Accordingly, with the knowledge of R_{TRSS}, an accurate thermo-mechanical simulation of the cooling process can be omitted, which is highly beneficial in reducing computational costs.

Previous works have indicated that the particle size and volume fraction [20,30–35] of PRMMCs affect R_{TRSS}. However, in previous investigations, the particles were often assumed to be spheres. In fact, real PRMMCs usually contain particles that have different ARs and align along the rolling or extrusion direction [10]. It has been pointed out that the morphology of the particles affects the residual stresses [23]. Therefore, to use Eq. (2) for predicting the tensile loading stress of PRMMCs, it is necessary to study the AR effect on TRSS and to calculate the value of R_{TRSS}. Then, this precomputed R_{TRSS} can be re-used afterwards for predicting the mechanical behavior of PRMMCs.

In this work, the representative volume elements (RVEs) with different particle ARs were analyzed using the FE method. To access R_{TRSS} via using Eq. (1), models with and without the cooling process were investigated. By comparing the R_{TRSS} obtained from FE models with various particle ARs, the influence of AR on TRSS of PRMMCs was studied. Based on the simulation results, the equivalent R_{TRSS} was found. Then, the simulation of the cooling process can be omitted. Instead, Eq. (2) can be used to take into account the effect of TRSS on strengthening mechanisms of PRMMCs, which reduces the computational costs significantly.

2. Computational approaches

2.1. Structures and boundary value problem

In this work, the PRMMCs with 17 vol.% particles were investigated. As shown in Fig. 1, four RVEs with the particle AR of 1, 2, 3, and 4 were created using the software *VirtualComposite-Pre* developed by the authors. Those RVEs were subjected to uniaxial tensile deformation to evaluate their mechanical properties. The loading direction (LD) was identical to the longitudinal direction of particles. Each RVE includes seven particles. Because the periodic structures were applied, particles near the surfaces of the RVEs were cut into parts. The size of each RVE is $100 \times 100 \times 100$ voxel^3. The voxel mesh is used as FE mesh. Therefore, the total element number is one million. Trilinear shape functions are introduced for the hexahedral element (C3D8 in Abaqus).

Periodic boundary conditions were employed, as illustrated in Fig. 2. The periodic boundary conditions on opposite boundary faces (Γ^t and Γ^b) are defined by:

$$u^t = u^a + u^b \tag{3}$$

where u^t and u^b are the displacement on faces Γ^t and Γ^b, respectively. The displacement u^a is a positive constant on the loading

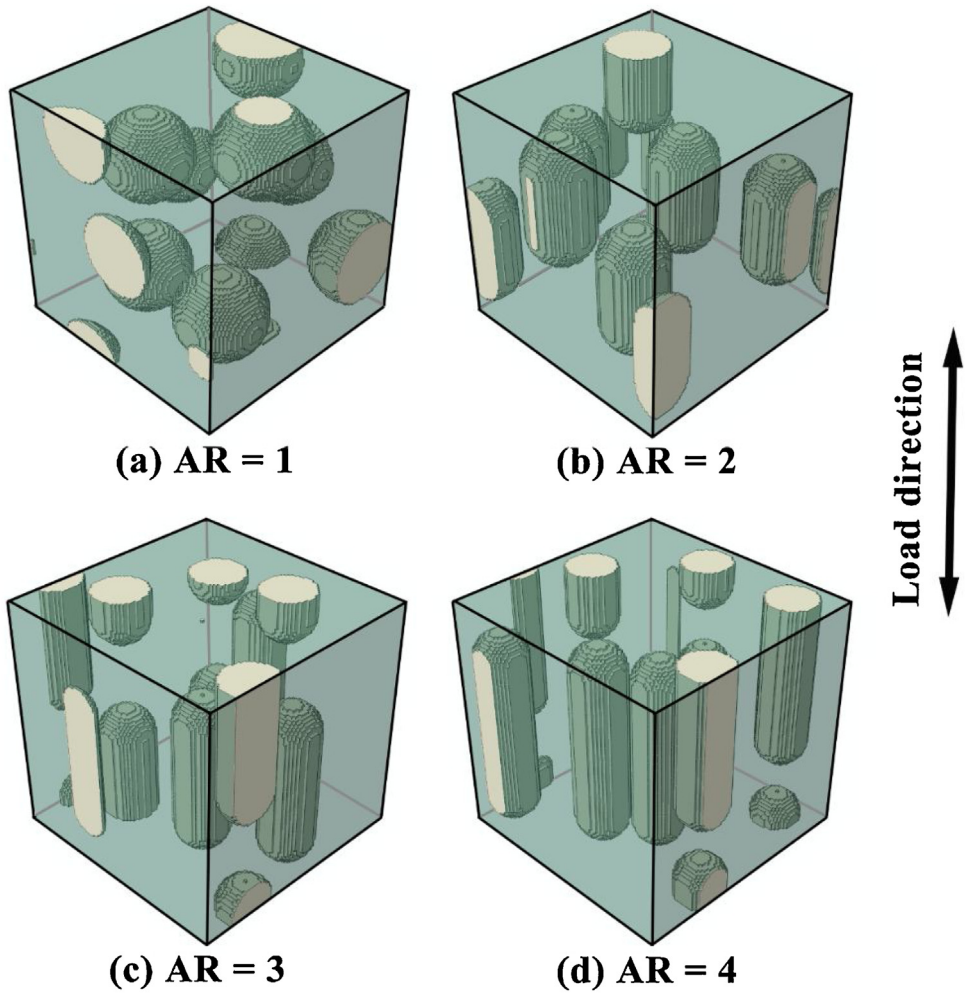

Fig. 1. RVEs of 17 vol.% PRMMCs with different ARs.

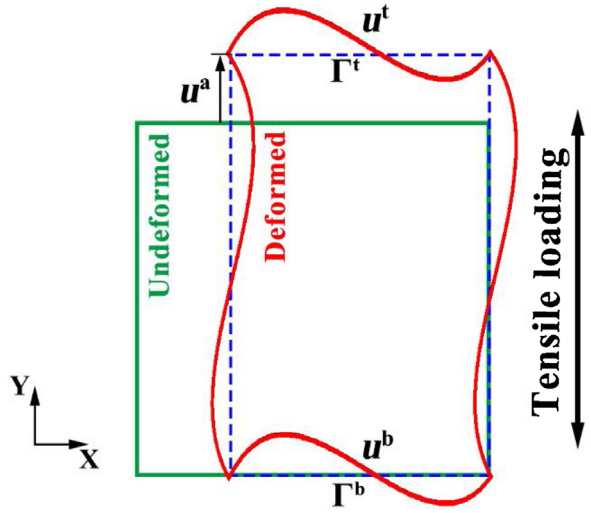

Fig. 2. Illustration of periodic boundary conditions.

faces to simulate the tensile loading. However, on all other free faces, the values of u^a are not fixed.

Then the effective strain and stress are calculated by:

$$\varepsilon_{\text{eff}} = u^a / L \tag{4}$$

$$\sigma_{\text{eff}} = F_R / L^2 \tag{5}$$

where L is the length of the cube-shaped RVE, F_R the reaction force on the loading surface and L^2 the area of the loading surface. To simulate uniaxial tensile deformation, u^a was set to 5% of L, which means that a 5% tensile strain was applied.

2.2. Material properties and cooling process

In this study, the material properties of the matrix and reinforcements were selected from the literature of typical PRMMCs (SiC/2009Al). The metal matrix in the composite was modeled as an elastoplastic material with isotropic hardening:

$$\sigma_y = \sigma_{y0}\left(1 + \frac{E\varepsilon_p}{\sigma_{y0}}\right)^N \tag{6}$$

where σ_y is the yield stress, σ_{y0} the initial yield stress, E the Young's modulus, ε_p the equivalent plastic strain and N a hardening parameter. In this study, N was assumed to be temperature independent and was set to 0.125 [28]. During tensile loading at room temperature, σ_{y0} was set to 300 MPa [10,36], which is the T4 condition of the alloy.

A quenching process was simulated before tensile loading to obtain TRSS. The quenching process was modeled as a cooling process from 515 °C to room temperature 25 °C. The temperature-dependent coefficients of thermal expansion (CTE), Young's modulus, and the initial yield strength of the matrix and reinforcement are specified as follows [28,37]:

$$\alpha_m = \left(-1.5\text{E}^{-11}T^2 + 1.6\text{E}^{-8}T + 2.2\text{E}^{-5}\right)\text{K}^{-1} \tag{7}$$

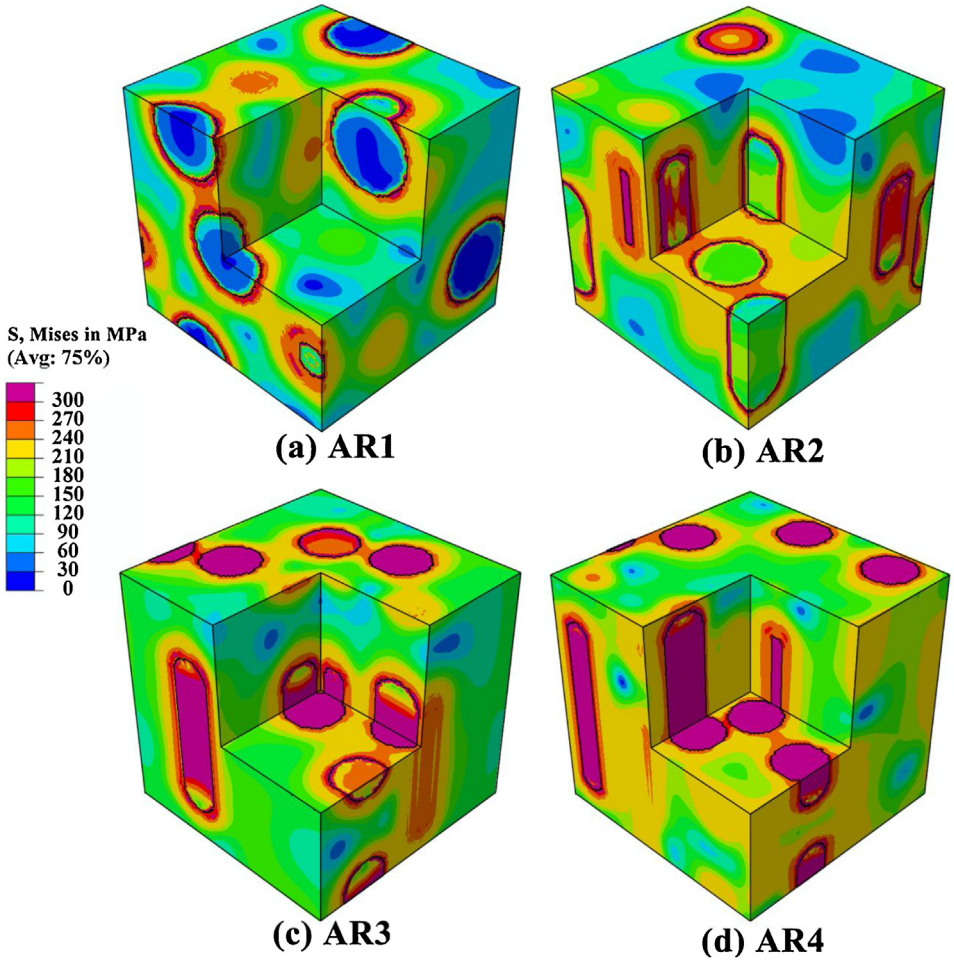

Fig. 3. Von Mises equivalent stress after the cooling process for different RVEs.

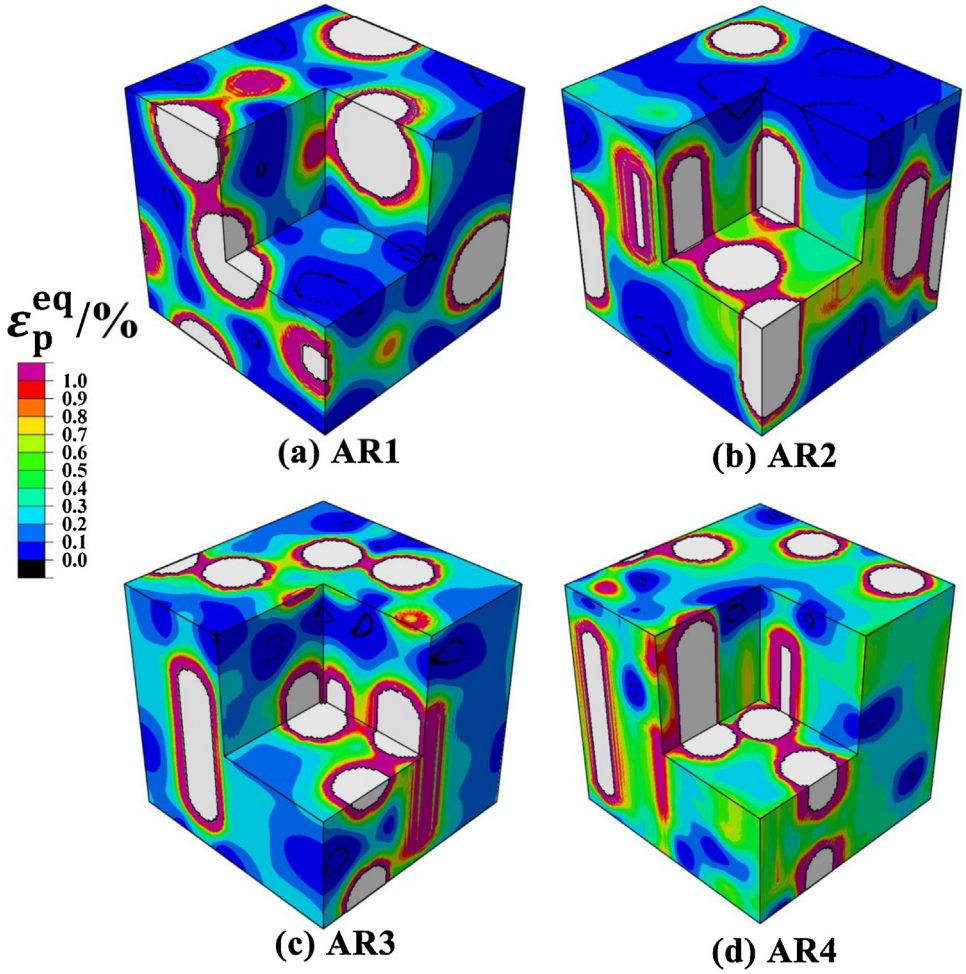

Fig. 4. Equivalent plastic strain after the cooling process for different RVEs.

$$\alpha_r = (-4.5\mathrm{E}^{-12}T^2 + 5.8\mathrm{E}^{-9}T + 3.1\mathrm{E}^{-6})\,\mathrm{K}^{-1} \tag{8}$$

$$E_m = \left(1.0\mathrm{E}^{-6}T^4 - 6.1\mathrm{E}^{-4}T^3 - 5.5\mathrm{E}^{-2}T^2 - 21.0T + 73655.0\right)\ \mathrm{MPa} \tag{9}$$

$$E_r = (-24.4T + 415115.0)\ \mathrm{MPa} \tag{10}$$

$$\sigma_{y0} = \begin{cases} \left(200.0 - 0.8E^{-1}T\right)\mathrm{MPa}, & 0.0\ ^\circ\mathrm{C} \le T \le 100.0\ ^\circ\mathrm{C} \\ (292.0 - T)\,\mathrm{MPa}, & 100.0\ ^\circ\mathrm{C} < T \le 265.0\ ^\circ\mathrm{C} \\ \left(41.4 - 5.8E^{-2}T\right)\mathrm{MPa}, & 265.0\ ^\circ\mathrm{C} < T \le 540.0\ ^\circ\mathrm{C} \end{cases} \tag{11}$$

where T is the temperature (°C), α the CTE, E the Young's modulus and σ_{y0} the initial yield stress of the matrix during the cooling process. Both the material properties of the matrix and reinforcements are assumed isotropic. In order to reflect the effect of room temperature aging, as shown in Eqs. (6) and (11), the initial yield stress σ_{y0} in room temperature is different during the tensile loading process and cooling process.

The calculated TRSS from the cooling process was considered as the initial state for the tensile loading simulation. Models without the cooling process were built and computed to assess the effect of TRSS. By comparing the difference between the models with and without the cooling process, the effect of TRSS can be evaluated quantitatively.

3. Computational results

3.1. AR effects on TRSS distribution

During the cooling process, the contraction difference between the particles and matrix along the LD is greater than that in other directions. The AR difference will lead to different contractions in three directions, which will lead to different stress states in the particles and the matrix. Fig. 3 shows the distribution of Mises stress in different RVEs after the cooling process. When AR equals 1, the particles are spheres, which causes that the stress state in particles is close to pure hydrostatic stress state. Therefore, the Mises stress in particles is exceptionally low. With increasing AR, the Mises stress in particles increases. Because the particles and the matrix have different CTE, the difference in deformation along the LD between the particles with higher AR and the matrix is larger, which leads to higher residual stress in both phases.

The incompatible contractions between the particles and the matrix cause plastic deformations in the matrix. Fig. 4 shows the equivalent plastic strain fields in the matrix. A higher AR obviously leads to higher plastic deformation in the matrix during the cooling process.

In Fig. 4(a) and (b), large plastic deformations occur near the particle/matrix interfaces, while plastic deformation in other zones is much smaller. In Fig. 4(c) and (d), plastic deformation occurs almost over the entire matrix with the highest values near the particle/matrix interfaces. For AR4, the equivalent plastic strain is much higher than other RVEs. During the cooling process, the deforma-

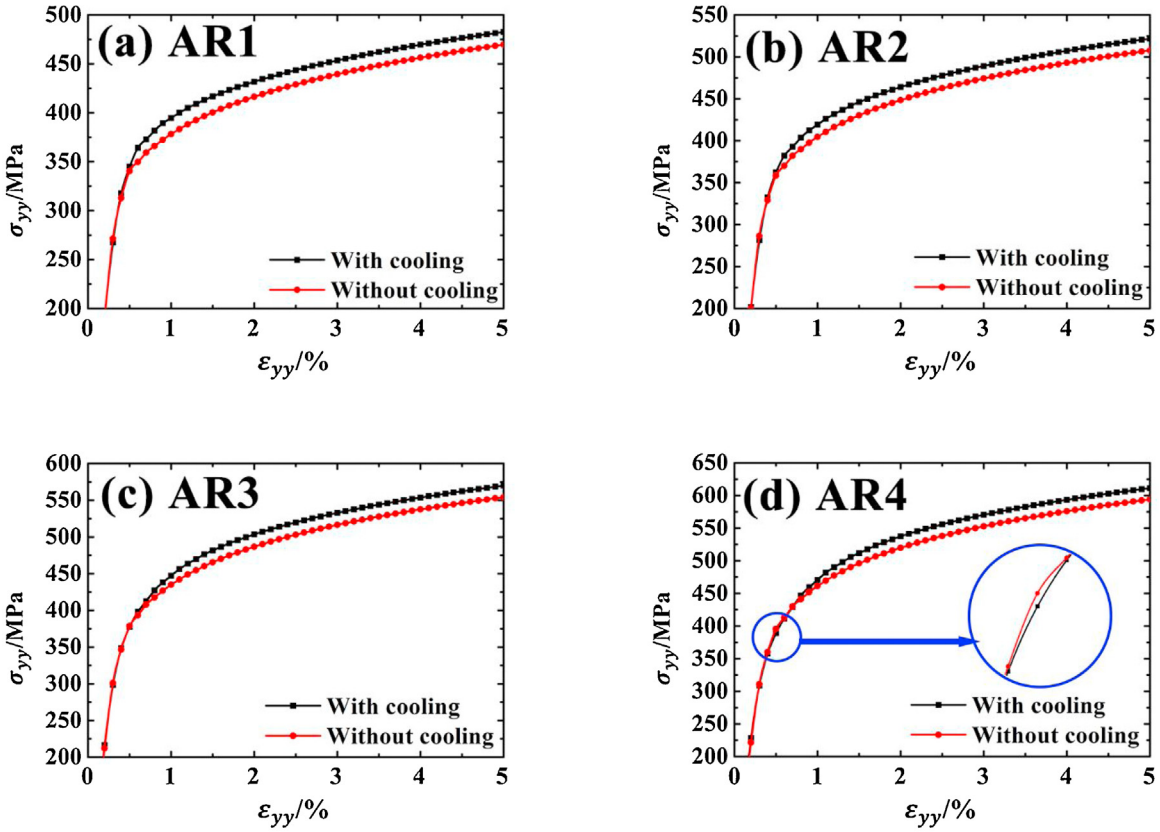

Fig. 5. Stress-strain curves for different RVEs with or without the cooling process.

tion of the particles is much less than that of the matrix ligament, which introduces tensile deformation in the matrix ligament, especially in the longitudinal direction of the particles. Therefore, with higher AR, the deformation mismatch between the two phases is more serious. The matrix alloy (2009Al) would undergo room temperature aging after quenching. The strain state after quenching causes dislocations in the matrix, which leads to pipe diffusion during aging [38,39]. The equivalent plastic strain after the cooling process in Fig. 4 can also help to analyze the pipe diffusion. However, the pip diffusion issue is not the topic of this work.

3.2. AR effects on predicted stress-strain curves

Because the tensile loading process of the composite is carried out after the cooling process, the residual stress and strain state of the composite after the cooling process is considered as an initial state. According to Section 3.1, AR affects TRSS. Therefore, it also affects the initial state of tensile loading. Fig. 5 shows the stress-strain curves predicted with or without the cooling process. According to the curves, the predicted yield stress with the cooling process is higher than that without the cooling process. Fig. 5(d) shows that the stress without the cooling process is slightly higher near the yield point, which coincides with the result in Refs. [20,37].

The differences between stress-strain curves predicted with and without the cooling process are shown in Fig. 6. At a strain of around 0.5%, the cooling process leads to a softening effect of about 5 MPa. Within the strain range of 0.5%-1.5%, the strengthening effect of TRSS decreases with increasing AR. However, beyond 1.5% strain, the strengthening effect increases with increasing AR. For all RVEs with different ARs, the strengthening effects have small variations at strains greater than 1.5%.

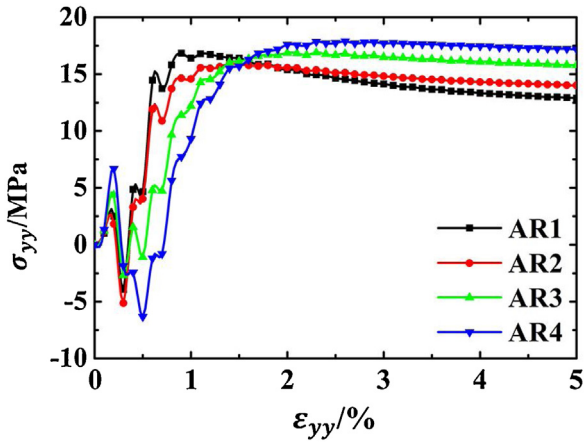

Fig. 6. Differences in stresses between cases with and without the cooling process.

3.3. Contribution ratio of TRSS

The evolutions of the contribution ratio of TRSS R_{TRSS} are shown in Fig. 7, which are calculated from Eq. (1) using the two sets of stress-strain data with and without the cooling process. The contribution ratio of TRSS is around -1.5% when the strain is around 0.5%. Within the strain range of 0.5%-1.5%, the contribution ratio of TRSS increases from around -1.5% to 3.5%. Beyond 1.5% strain, the contribution ratio of TRSS is around 3.5% and decreases slightly with strain. When the strain is smaller than 0.5%, the contribution ratio of TRSS shows high fluctuation and independence of AR values. To obtain a simple expression of R_{TRSS}, if the strain is smaller than 0.5%, the contribution ratio R_{TRSS} in Eq. (1) were set as the average of all R_{TRSS} in that region.

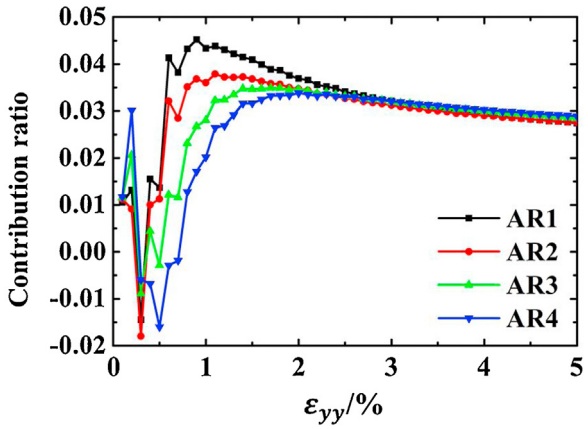

Fig. 7. Contribution ratio evolution of TRSS during tensile loading.

For realistic PRMMCs [10], it is very common that the ARs of particles ranges from 1–4. Therefore, the average R_{TRSS} obtained from Fig. 7 with ARs of 1–4 can be used as an effective contribution ratio of TRSS in Eq. (2). The regression function of the average R_{TRSS} is:

$$R_{avg} = \begin{cases} 0.005, & 0.000 \le \varepsilon < 0.005 \\ -0.022 + 5.380\varepsilon, & 0.005 \le \varepsilon < 0.010 \\ 0.032 - 0.095\varepsilon, & 0.010 \le \varepsilon < 0.050 \end{cases} \quad (12)$$

If the ARs of particles are not distributed uniformly, then the R_{avg} can be obtained using relative weight for each AR. Using this function R_{avg}, it is possible to introduce the influence of TRSS on the stress-strain curves of 17 vol.% PRMMCs in an efficient way. This method is also applicable to introduce the TRSS effect for other PRMMCs.

3.4. Application of the contribution ratio of TRSS

To verify that the influence of TRSS can be introduced by using Eq. (2), another RVE with four different ARs of particles was designed. As shown in Fig. 8(a), this RVE has 12 particles inside. For each AR, three particles are inside. The size of the RVE is 120 × 120 × 120 voxel^3, and the volume fraction of particles is 17 %.

Two uniaxial tensile tests with and without the cooling process were simulated. As shown in Fig. 8(b), the yield stress obtained from simulation with the cooling process is higher than that without the cooling process, which is coincident with the results in Fig. 5. Using Eq. (2) and the stress-strain curve without the cooling process, a new curve was obtained (new method). The R_{avg} in Eq. (12) was taken as the effective R_{TRSS}. The simulations with and without the cooling process were all carried out on the same computer (CPU: Xeon E5-2630 v3) using 20 threads. However, the simulation with the cooling process cost 145 h, while the simulation without the cooling process only cost 71 h. Because the new method only needs to combine the stress-strain curve without the cooling process and Eq. (2) together, it cost the same computational time as the simulation without the cooling process. As shown in Fig. 8(b), the stress-strain curves of the new method and with the cooling process are almost coincident.

In summary, the new method is verified to introduce the influence of TRSS on the stress-strain curves of PRMMCs. Besides, the new method has reduced the computational cost by a factor 2. Because it is difficult to find a PRMMC without TRSS, using experimental data to verify the method is challenging. Therefore, the new method was only verified by comparing the numerical results.

4. Discussion

4.1. Pre-yield effects of TRSS

As shown in Fig. 4, plastic deformation has already occurred in the matrix after the cooling process but before the tensile loading. This phenomenon was defined as the "pre-yield effect of TRSS". RVEs with different ARs show pre-yield effects with different levels. As shown in Fig. 7, within the strain range of 0.5%-1.5%, RVEs with higher particle ARs show a smaller contribution ratio of TRSS. It indicates that a higher AR leads to the smaller strengthening effect of TRSS because a higher AR leads to earlier yield and larger plastic strain in the matrix, as shown in Fig. 4.

The volume fraction of the plastic zone is assessed to investigate the influence of AR on this pre-yield effect, which is calculated by:

$$f_p = \frac{V_{mp}}{V_m} \quad (13)$$

where f_p is the volume fraction of the plastic zone in the matrix. The volume of the matrix that already yielded is denoted by V_{mp}, and V_m is the entire volume of the matrix. Because the temperature and yield stress of the matrix were changing during the cooling process, the zone experienced plastic deformation during the cooling process may not yield at the beginning of the tensile loading process at room temperature. Therefore, the volume fraction of the plastic zone in the matrix is not 100% at the beginning of the tensile load-

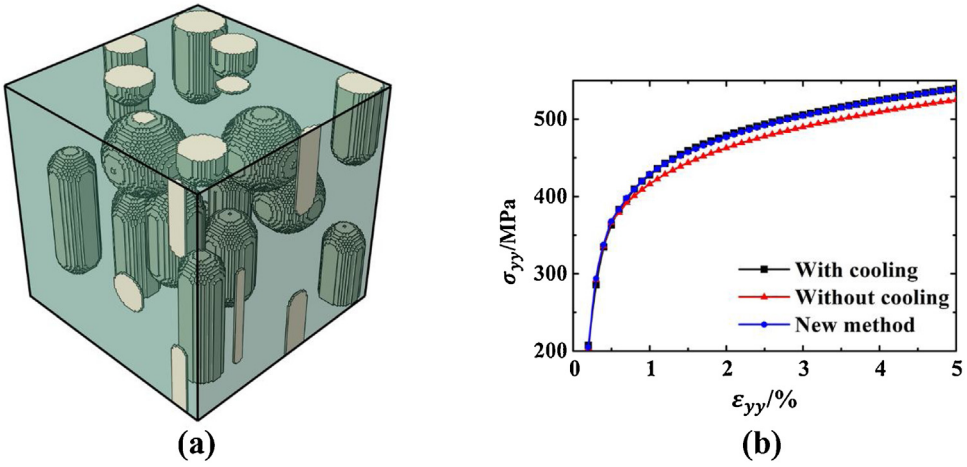

Fig. 8. Verification of using Eq. (2) to introduce the influence of TRSS on the stress-strain curves of PRMMCs. (a) The RVE of 17 vol.% PRMMCs with four different ARs of particles. (b) The stress-strain curves obtained from simulations with the cooling process, without the cooling process, and using the new method.

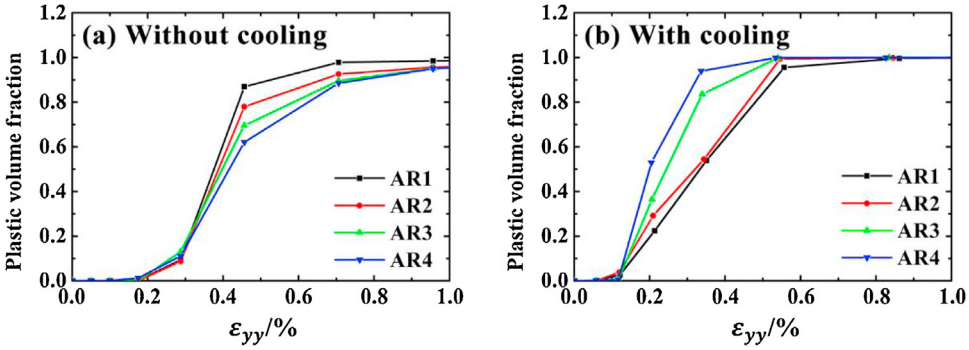

Fig. 9. Plastic volume fraction of the matrix as a function of strain for different RVEs.

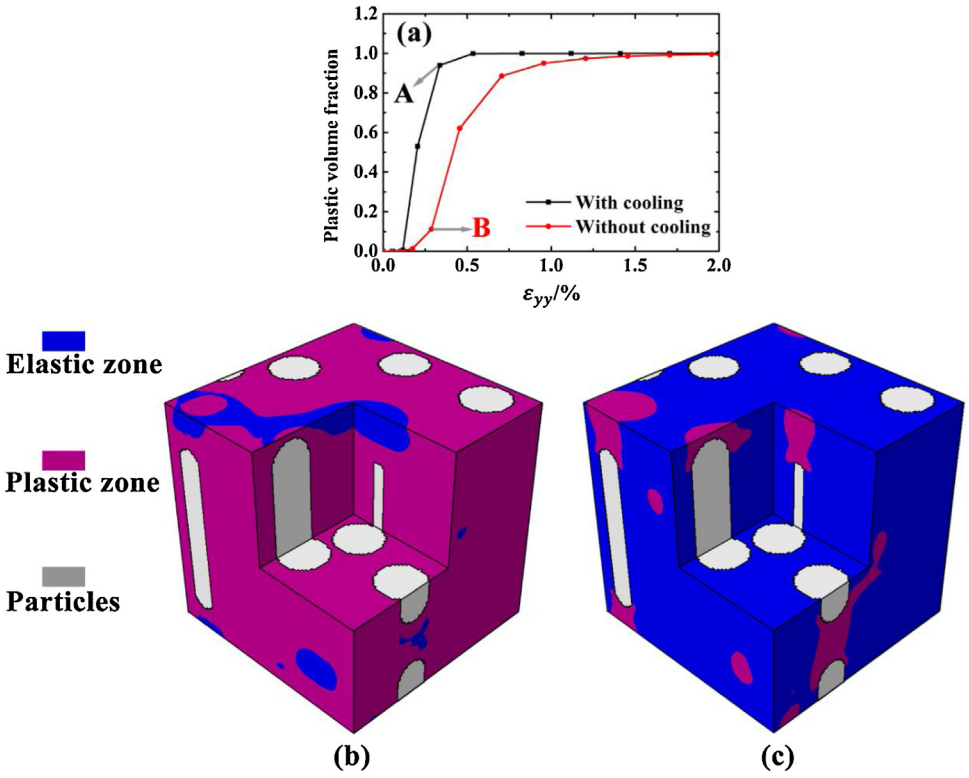

Fig. 10. Plastic deformation of AR4 with and without the cooling process. (a) Evolution of plastic volume fraction, (b) distribution of plastic zone at point A in (a), (c) distribution of plastic zone at point B in (a).

ing process, even though almost all the matrix experienced plastic deformation, according to Fig. 4.

Fig. 9 shows the evolution of f_p with strain growing from 0 to 1%. The results obtained from models with and without the cooling process show an opposite variation trend with changing AR of particles. Without the cooling process, a higher AR leads to a lower f_p at the same strain value. On the contrary, with the cooling process, a higher AR leads to a greater f_p at the same strain value. Without the cooling process and at the same strain value, the matrix with a higher AR retains a larger elastic zone. However, with the cooling process and at the same strain value, the matrix exhibits a larger plastic zone in the composite with higher AR particles. During the tensile loading, with the same increment of strain, the stress increment of the plastic zone is less than that of the elastic zone. This indicates that the pre-yield effect changes the stress-strain behavior of the matrix in the composite. In the composite with higher AR particles, the change of f_p starts earlier and more strongly when considering the cooling process. Therefore, when the tensile strain is between 0.5% and 1.5%, the contribution ratio of TRSS decreases with AR increment, as shown in Fig. 7. When the tensile strain is above 1.5%, all the matrix zone yields and experiences plastic deformation; the pre-yield effect does not influence the contribution ratio of TRSS anymore.

Fig. 10(a) compares f_p of the RVE AR4 with and without the cooling process. As shown in Fig. 3(d), high stress is exhibited in the matrix before tensile loading. Therefore, at a similar applied strain, the plastic zone in the model with the cooling process is much larger than that in the model without the cooling process, as shown in Fig. 10(b) and (c).

4.2. Fiber-reinforced metal matrix composite

In this work, PRMMCs with different ARs were investigated. If AR is increased to an extreme situation, fiber-reinforced metal matrix composite will be obtained. This section discusses the influence of TRSS in fiber-reinforced metal matrix composite.

As shown in Fig. 11(a), an RVE with 7 fibers was built. The volume fraction of the reinforcement was also 17%. The contribution ratio

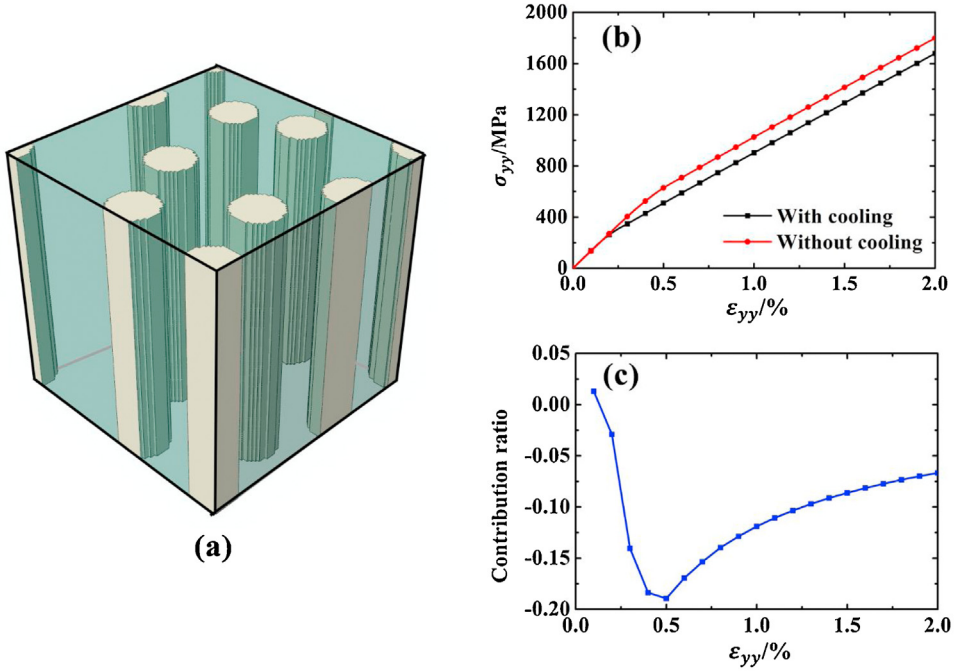

Fig. 11. Continuous fibers reinforced composite with 17 vol.% fibers. (a) the RVE model, (b) stress-strain curves obtained from simulations, and (c) contribution ratio of TRSS during tensile loading.

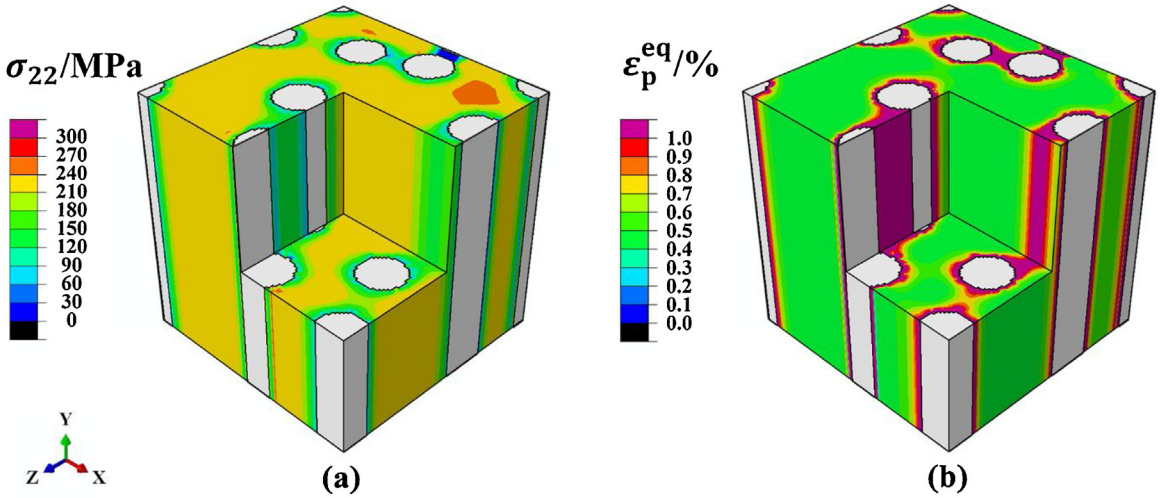

Fig. 12. Fields of (a) the stress component along the loading direction and (b) equivalent plastic strain ε_p^{eq} in the matrix after the cooling process.

of TRSS in this model was shown in Fig. 11(b). The contribution ratio of TRSS is less than 0 during almost the entire tensile loading process. The TRSS has a softening effect on fiber-reinforced metal matrix composite.

Fig. 12(a) shows the distribution of stress along the LD after the cooling process. Compared to that in PRMMCs, the cooling process causes a more pronounced and earlier pre-yield effect in the metal matrix. As shown in Fig. 12(b), in fiber-reinforced composite, the thermal residual plastic strain is much higher than PRMMCs.

4.3. Limitations

This study showed the effect of AR on the TRSS of PRMMCs. Using the average contribution ratio of TRSS, the stress-strain curve of 17 vol.% PRMMCs with an average distribution of particles AR was obtained. For 17 vol.% PRMMCs with a different distribution of particles AR, the average contribution ratio of TRSS can be obtained based on the number of particles of each AR. However, for different volume fractions, reinforcement and matrix, the contribution ratios of TRSS need to be recalculated. And because of the strong pre-yield effect of fiber-reinforced metal matrix composite, this method is not suitable for PRMMCs with too high AR.

5. Conclusions

In this work, quenching and tensile loading behaviors of PRMMCs with four different ARs were simulated to study the effect of AR on TRSS. The following conclusions can be drawn:

(1) When the tensile strain is between 0.5% and 1.5%, a higher AR leads to a lower strengthening effect of TRSS. When the ten-

sile strain is greater than 1.5%, a higher AR leads to a higher strengthening effect due to TRSS.

(2) Around a tensile strain of 0.5%, TRSS can even lead to a slight softening effect. The pre-yield effect of the metal matrix caused by TRSS is the reason for this softening effect. The pre-yield effect is strong in fiber-reinforced metal matrix composite, which leads to a softening effect during the entire tensile loading process.

(3) The average contribution ratio of TRSS has been calculated. The effect of TRSS can be included in the predicted yield stress without simulating the cooling process of PRMMCs using the fitted contribution ratio, which reduces the computational costs significantly.

Declaration of Competing Interest

The authors declare that they have no known competing financial interests or personal relationships that could have appeared to influence the work reported in this paper.

Acknowledgements

This work was financially supported by the National Key R&D Program of China (No. 2017YFB0703104), the Key Research Program of Frontier Sciences, CAS (No. QYZDJ-SSW-JSC015), the National Natural Science Foundation of China (Nos.51931009, 51871214 and 51871215) and the Youth Innovation Promotion Association CAS (No.2020197).

References

[1] T.W. Clyne, P.J. Withers, An Introduction to Metal Matrix Composites, Cambridge University Press, New York, 1995.
[2] Y.N. Zan, Y.T. Zhou, H. Zhao, Z.Y. Liu, Q.Z. Wang, D. Wang, W.G. Wang, B.L. Xiao, Z.Y. Ma,Compos. Part B: Eng. 183 (2020), 107674.
[3] L.J. Huang, L. Geng, H.X. Peng, Prog. Mater. Sci. 71 (2015) 93–168.
[4] Y.N. Zan, Q. Zhang, Y.T. Zhou, Z.Y. Liu, Q.Z. Wang, D. Wang, B.L. Xiao, W.C. Ren, Z.Y. Ma, Compos. Part B: Eng. 195 (2020) 1–10.
[5] T. Han, E. Liu, J. Li, N. Zhao, C. He, J. Mater. Sci. Technol. 46 (2020) 21–32.
[6] L. Huang, Q. An, L. Geng, S. Wang, S. Jiang, X. Cui, R. Zhang, F. Sun, Y. Jiao, X. Chen,Adv. Mater. (2020), 2000688.
[7] X.X. Zhang, L.H. Wu, H. Andrä, W.M. Gan, M. Hofmann, D. Wang, D.R. Ni, B.L. Xiao, Z.Y. Ma, J. Mater. Sci. Technol. 35 (2019) 824–832.
[8] X. Gao, L. Yuan, Y. Fu, X. Yao, H. Yang,Compos. Part B: Eng. 197 (2020), 108164.
[9] X.X. Zhang, J.F. Zhang, Z.Y. Liu, W.M. Gan, M. Hofmann, H. Andrä, B.L. Xiao, Z.Y. Ma, J. Mater. Sci. Technol. 54 (2020) 58–68.
[10] J.F. Zhang, X.X. Zhang, Q.Z. Wang, B.L. Xiao, Z.Y. Ma, Mech. Mater. 122 (2018) 96–103.
[11] Y. Song, Y. Ma, K. Zhan,Mech. Mater. 142 (2020), 103283.
[12] L. Zhou, C. Cui, Q.Z. Wang, C. Li, B.L. Xiao, Z.Y. Ma, J. Mater. Sci. Technol. 34 (2018) 1730–1738.
[13] X. Gao, X. Zhang, L. Geng, Mater. Sci. Eng. A 740–741 (2019) 353–362.
[14] P. Peng, M. Gao, E. Guo, H. Kang, H. Xie, Z. Chen, T. Wang,Mater. Sci. Eng. A 781 (2020), 139169.
[15] X. Niu, H. Zhang, Z. Pei, N. Shi, C. Sun, J. Gong, J. Mater. Sci. Technol. 35 (2019) 88–93.
[16] C. Li, X. Si, J. Cao, J. Qi, Z. Dong, J. Feng, J. Mater. Sci. Technol. 35 (2019) 2470–2476.
[17] N. Ramakrishnan, Acta Mater. 44 (1996) 69–77.
[18] Y.B. Zhang, T. Andriollo, S. Fæster, R. Barabash, R. Xu, N. Tiedje, J. Thorborg, J. Hattel, D. Juul Jensen, N. Hansen, Acta Mater. 167 (2019) 221–230.
[19] R. Fernández, S. Cabeza, T. Mishurova, P. Fernández-Castrillo, G. González-Doncel, G. Bruno, Mater. Sci. Eng. A 731 (2018) 344–350.
[20] D. Cao, Q. Duan, S. Li, Y. Zhong, H. Hu, Compos. Struct. 200 (2018) 290–297.
[21] N.K. Sharma, R.K. Mishra, S. Sharma, Comput. Mater. Sci. 115 (2016) 192–201.
[22] O. Pierard, J. LLorca, J. Segurado, I. Doghri, Int. J. Plast. 23 (2007) 1041–1060.
[23] H.J. Böhm, A. Rasool, Int. J. Solids Struct. 87 (2016) 90–101.
[24] F. Bouafia, B. Serier, B.A.B. Bouiadjra, Comput. Mater. Sci. 54 (2012) 195–203.
[25] S. Amir-Ahmadi, A.R. Ghasemi, M. Mohammadi,Mech. Mater. 136 (2019), 103083.
[26] H.K. Park, J. Jung, H.S. Kim, Comput. Mater. Sci. 126 (2017) 265–271.
[27] A. Jafarpour, M. Safarabadi Farahani, M. Haghighi-Yazdi,Mech. Mater. 138 (2019), 103176.
[28] J.F. Zhang, H. Andrä, X.X. Zhang, Q.Z. Wang, B.L. Xiao, Z.Y. Ma,Compos. Struct. 226 (2019), 111281.
[29] J. Xu, Y. Li, K. Ma, Y. Fu, E. Guo, Z. Chen, Q. Gu, Y. Han, T. Wang, Q. Li, Scr. Mater. 187 (2020) 142–147.
[30] M. Taya, K.E. Lulay, D.J. Lloyd, Acta Metall. Mater. 39 (1991) 73–87.
[31] J.C. Shao, B.L. Xiao, Q.Z. Wang, Z.Y. Ma, K. Yang, Compos. Sci. Technol. 71 (2011) 39–45.
[32] A.S. Bouchikhi, Mater. Des. 31 (2010) 2091–2096.
[33] F. Teixeira-Dias, L.F. Menezes, Comput. Mater. Sci. 21 (2001) 26–36.
[34] S. Majumdar, D. Kupperman, J. Am. Ceram. Soc. 72 (1989) 312–313.
[35] K. Seol, A.D. Krawitz, J.W. Richardson, C.M. Weisbrook, Mater. Sci. Eng. A 398 (2005) 15–21.
[36] J.F. Zhang, X.X. Zhang, Q.Z. Wang, B.L. Xiao, Z.Y. Ma, J. Mater. Sci. Technol. 34 (2018) 627–634.
[37] X.X. Zhang, B.L. Xiao, H. Andrä, Z.Y. Ma, Compos. Struct. 137 (2016) 18–32.
[38] M. Garbrecht, B. Saha, J.L. Schroeder, L. Hultman, T.D. Sands, Sci. Rep. 7 (2017) 46092.
[39] C. Rockenhäuser, S. Schriever, P. von Hartrott, B. Piesker, B. Skrotzki, Mater. Sci. Eng. A 716 (2018) 78–86.